Iranian Journal of Chemical Engineering
Vol. 8, No. 2 (Spring), 2011, IAChE

Convective Heat Transfer of Nanofluids Flows Through an Isothermally Heated Curved Pipe

E. Ebrahimnia-Bajestan, H. Niazmand[*]
Mechanical Engineering Department, Ferdowsi University of Mashhad, Mashhad, Iran

Abstract

In the current study, numerical simulation of laminar flow and heat transfer of water mixture with carbon nanotubes (CNT) as nanofluids in a 90 degree curved pipe are considered. The incompressible Navier-Stokes and energy equations are solved numerically in a body fitted coordinates system using a control volume technique. An interfacial layer-based model is applied to predict the thermal conductivity of nanofluid. The axial velocity contours, secondary flow patterns and temperature fields for different values of the particles concentrations are examined in detail. Furthermore, the effects of nanoparticles concentration on the heat transfer are studied. The results indicate that due to the secondary flows induced by curvature effects, the heat transfer rate is improved, and enhanced remarkably further using nanofluids. Furthermore, the nanoparticles, especially at higher concentration levels, generate more uniform cross sectional temperature distributions.

Keywords: *Numerical Study, Curved Pipe, Nanofluid, Carbon Nanotubes, Convective Heat Transfer*

1- Introduction

The performance of heat exchangers can be improved by heat transfer enhancement techniques, which are, in general, divided into two main groups: active and passive [1]. The active techniques require external forces, e.g. electric field, acoustic or surface vibration, etc, while in passive techniques fluid additives such as nanoparticles or special flow geometries such as curved tubes are employed.

Curved tubes, as one of the passive heat transfer enhancement techniques, have been widely used in heat transfer applications. The flow pattern in curved tubes is more complex than that in straight tubes, since fluid motion in a bend is not parallel to the curved axis of the bend. As the flow enters the bend, the centrifugal forces act outward from the center of the curvature on the fluid particles. Therefore, the slower moving fluid particles travel along paths with smaller radii of curvatures than those of the faster moving particles. This leads to the onset of a secondary flow such that fluid nearer the wall moves toward the inner wall while fluid

∗ Corresponding author: Hniazmand@yahoo.com

in the core region moves to the outer wall. The existence of a secondary flow field, which is superimposed upon the axial velocity flow field, causes the transfer processes to enhance such as heat and mass.

On the other hand, the inherently poor thermophysical properties of conventional heat transfer fluids such as water, ethylene glycol or engine oil greatly limit the heat transfer performance of heat exchangers. There are various solids which possess the thermal conductivity more than one order-of-magnitude higher than fluids. For example, the thermal conductivity of aluminum oxide at room temperature is about 67 times greater than that of water and about 275 times greater than that of engine oil. Therefore, the thermal conductivities of fluids containing suspension of these millimeter or micrometer solid particles are expected to be significantly higher than those of conventional heat transfer fluids. The main problems of these suspensions, such as poor suspension stability, channel clogging, extra pressure drop and erosion have limited their application.

In contrast to micrometer size particles suspension, nanofluids, which are suspensions of nanoparticles in conventional fluids, are very stable and almost free from the mentioned problems [2]. Nanofluids have attracted great interest due to their potential benefits and applications in important fields such as microelectronics, energy supply, transportation, HVAC and biomedical [3].

Previous studies have shown that even for low volume fractions of nanoparticles, the measured thermal conductivity of nanofluids is about one order of magnitude higher than that predicted by classical theory [4]. In the past decade, considerable efforts have been made to develop theories and models that properly account for the enhanced thermal conductivity of nanofluids. A number of researchers have proposed that one of the major mechanisms behind the anomalous thermal conductivity enhancement of nanofluids is the layering of liquid molecules at the solid-particle interface, which is commonly referred to as the interfacial layer or nanolayer [5-8]. The atomic structure of this liquid layer is significantly more ordered than that of bulk liquid and therefore the thermal conductivity of this nanolayer would be expected to be higher than the bulk liquid [6]. Therefore, this solid-like nanolayer increases the heat transfer between the solid nanoparticle and the bulk liquid [4]. In addition, the interfacial layer thickness results in a larger effective volume fraction of the particle-layered-liquid structure, which would tend to enhance the thermal conductivity [3].

Several models have been proposed to consider the effect of this interfacial layer in the prediction of nanofluids heat transfer behavior [3-7]. These models are generally semi-empirical since there is no available expression for calculating the thickness and conductivity of the nanolayer. The thickness of this layer of liquid molecules at the interface is at a magnitude of nanometer. Also, the nanolayer would be expected to have an intermediate thermal conductivity between the bulk liquid and the nanoparticle. In these models, the thickness and conductivity of the ordered layer are chosen such that the calculated thermal conductivity matches the measured values of the nanofluid thermal conductivity. Most of these models

are for spherical nanoparticles. Among them, Murshed et al. [5] have presented a model for cylindrical nanoparticles such as carbon nanotubes (CNTs).

Several experimental investigations have shown that nanofluids not only have a better thermal conductivity, but also have a higher convective heat transfer capability than the base fluids [8-17]. Also, the experimental evidence indicates that nanofluids heat transfer coefficients are increased more than what is expected just from thermal conductivity enhancement in both laminar and turbulent flows [2]. Therefore, several mechanisms have been proposed to account for the convection heat transfer enhancement [13, 18].

Besides the experimental researches, there are some numerical works on convective heat transfer of nanofluids [19-33]. The results have shown that the nanofluids can improve the heat transfer characteristics, and these enhancements are augmented with increasing in nanoparticles volume fractions. These numerical investigations help to get a better understanding of flow and heat transfer mechanisms in nanofluids to present proper models for convective heat transfer coefficients. The numerical solutions can be applied to simulate the convective heat transfer of various nanofluids at different flow geometries and boundary conditions. Numerical researchers have studied different types of nanoparticles, such as Al_2O_3 [19-29], Cu [26, 30], CNT [31] and TiO_2 [32]. Most of these numerical investigations are related to straight pipes [21-23, 26-28, 30 -32]. Moreover, there is limited information available on the flow pattern and heat transfer of nanofluids in curved pipes [20, 24, 25, 29].

Akbarinia et al. [20, 24, 25] studied the mixed convective heat transfer of nanofluids in the 180° curved pipe, numerically. Their results indicated that nanofluids have positive effects on heat transfer enhancements in curved pipes. Recently, Ebrahimnia-Bajestan et al. [29] compared the thermal effects of forced convective heat transfer of nanofluids in straight and curved pipes. They showed that both the nanoparticle and curvature effects enhance heat transfer characteristics. It is worth mentioning that to the best of the authors knowledge, experimental study of nanofluids in curved pipes is not available. Furthermore, in most of the published numerical and experimental works the constant wall heat flux condition is employed and the constant wall temperature studies are rather limited [30].

Nanofluids flows can be modeled as either single phase or two phase flows. In single phase approach it is assumed that the based fluid and nanoparticles are in thermal and hydrodynamic equilibrium and the presence of the nanoparticles is accounted for by introducing the effective thermophysical properties for the nanofluid [19, 20, 23-28]. Single phase approach is more common than the two phase model, where nanofluid is considered as two separate phases of liquid and solid nanoparticles [21, 22] due to its simplicity in modeling and the lower cost of the computations.

The above review reveals the need for further studies in identifying the basic characteristics associated with the transfer behavior of the nanofluids. In particular, there are very few works on thermal conductivity modeling and convective heat transfer characteristics of nanofluids containing CNTs. In this research,

two passive techniques of heat transfer enhancement, curvature effects and nanofluids, are studied. Laminar flow and heat transfer of nanofluids consist of CNTs in water in a 90 degree curved pipe with constant wall temperature boundary condition considered. The density and heat capacity of the mixtures are computed based on the classical two-phase mixture models. The dynamic viscosity of nanofluids is obtained by performing a least-squares curve fitting to the available experimental data in literature. An interfacial layer-based model is applied to predict the thermal conductivity of nanofluids. The incompressible Navier-Stokes and energy equations are solved numerically in a body fitted coordinates system using a control volume technique. The axial velocity variations, secondary flow patterns and temperature profiles for different values of the particles concentrations are examined in detail. Furthermore, the effects of nanoparticles concentration on the Nusselt number and the overall heat transfer rates are discussed.

2- Mathematical modeling

Figure 1 shows the geometry of the problem consists of a 90^o curved circular pipe with two straight sections at both ends. The straight pipe at the curved inlet is four diameters long, while it extends to six diameters at the curved exit. The radius of curvature, along with the location of some selected cross sections where the results will be discussed, are also shown in this figure.

It is assumed that the fluid phase and nanoparticles are in thermal equilibrium with zero relative velocity. The governing equations for laminar incompressible flows cast in integral form, which is more suitable for the control volume approach, are described as:

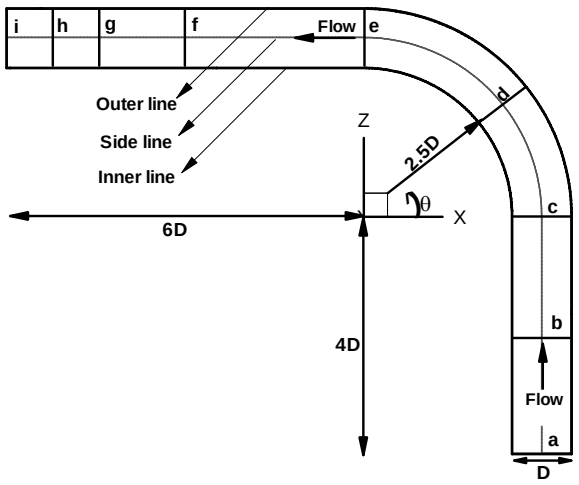

Figure 1. Flow geometry and the locations of the important cross sections and lines

$$\iint \rho_e \vec{V} \cdot d\vec{A} = 0 \tag{1}$$

$$\int_{\forall} \rho_e \frac{\partial \vec{V}}{\partial t} d\forall + \iint \vec{V} \rho_e \vec{V} \cdot d\vec{A} = -\iint p\vec{n} \cdot d\vec{A} + \iint \mu_e \vec{\nabla} \vec{V} \cdot d\vec{A} \tag{2}$$

$$\int_{\forall} (\rho C_p)_e \frac{\partial T}{\partial t} d\forall + \iint (\rho C_p)_e T\vec{V} \cdot d\vec{A} = \iint k_e \vec{\nabla} T \cdot d\vec{A} \tag{3}$$

where $\vec{V}$, p and T are the velocity vector, pressure, and temperature. Vectors $\vec{A}$ and $\vec{n}$ represent the cross-sectional area and its normal unit vector, respectively. Also, ρ_e, k_e, μ_e, C_{p_e} are density, thermal conductivity, viscosity and heat capacity of nanofluid, respectively, where the subscript e indicates effective properties of nanofluids defined as:

Density:

$$\rho_e = (1-\phi)\rho_f + \phi\rho_p \tag{4}$$

Heat capacity:

$$C_{p_e} = \frac{(1-\phi)(\rho C_p)_f + \phi(\rho C_p)_p}{(1-\phi)\rho_f + \phi\rho_p} \tag{5}$$

The dynamic viscosity of CNT/water nanofluid is obtained by a least-square curve fitting to the experimental results of [33] expressed by:

$$\frac{\mu_e}{\mu_f} = (1 + 22.7814\phi - 9748.4\phi^2 + 1000000\phi^3) \tag{6}$$

where ϕ is the volume fraction of the nanoparticles. Equation (6) is applicable for the CNTs volume fractions less than 1%.

The static mechanism-based model as described in [5] is adopted for the prediction of effective thermal conductivity of nanofluids having cylindrical nanoparticles. According to this model the effective thermal conductivity of water and CNTs (cylindrical nanoparticles) mixture is expressed by:

$$\begin{aligned} k_e = [&(k_p - k_l)\phi\, k_l(\gamma_1^2 - \gamma^2 + 1) + (k_p + k_l)\gamma_1^2 \\ &\times (\phi\gamma^2(k_l - k_f) + k_f)][\gamma_1^2(k_p + k_l) \\ &- (k_p - k_l)\phi(\gamma_1^2 + \gamma^2 - 1)]^{-1} \end{aligned} \tag{7}$$

where k_p and k_f is the nanoparticles and fluid thermal conductivity, respectively. For a cylindrical nanoparticle with radius a and the interfacial layer l between particle/fluid with thickness h and thermal conductivity k_l, parameters γ and γ_1 are defined as: $\gamma = 1 + h/a$, $\gamma_1 = 1 + h/2a$.

As mentioned earlier, these models are semi-empirical and therefore, the unknown thickness and conductivity of the ordered layer have to be chosen such that the calculated effective thermal conductivities match the measured values. In the present study, the interfacial layer thickness of 2 nm for CNTs is adopted according to the Murshed et al. study [5]. Furthermore, for the CNT /water the present thermal conductivity model fitted well with the results of [33], if k_l is set to $k_l = 555 \times k_f$. In this investigation, the CNTs are 15nm in diameter and 30μm in height, with a volume fraction lower than 1%. It is clear that the computed thermal conductivity of the interfacial layer is considerably larger than the thermal conductivity of the based fluid.

As for boundary conditions, parabolic velocity profile is assumed at the inlet, while zero gradients are applied for all variables at the outlet. The inlet temperature of T_i = 293.15K and the constant wall temperature of T_w = 363.15K are considered.

The numerical solution is based on a projection-type method which solves the flow field in two steps. First, an intermediate velocity field is obtained using the available pressure field. Next, velocity and pressure corrections are calculated from a Poison equation designed to satisfy the continuity equation. The numerical scheme was originally developed by Chorin [34] and improved further by Dwyer [35] and the present authors [36]. Following Dwyer et al.

[37] a new pressure correction is employed to improve the convergence performance of the Poisson equation solver. The correction is based on the physical considerations of preserving the mass flow rate at each cross section for incompressible flows. Therefore, a streamwise pressure gradient is introduced to make up for the local velocity defect as:

$$-\frac{\partial p'}{\partial s} = \rho \frac{\Delta U_k}{\Delta t} \tag{8}$$

where s is the streamline direction and the local velocity defect at each cross section is defined as:

$$\Delta U_k = U_i - \frac{\iint_A \vec{V} \cdot d\vec{A}}{A} \tag{9}$$

where A is the pipe cross sectional area and U_i is the inlet averaged velocity. This pressure correction is added to the pressure correction obtained from the continuity equation and the solution procedure continues until the converged results are obtained. Clearly, when the mass is conserved at each cross section this pressure correction vanishes.

Extensive computations have been performed to identify the number of grid points that produces reasonably grid independent results. It was found that the minimum grid points of 42 ×41 × 251 are required in the azimuthal, radial, and axial directions, respectively. Uniform grid spacing is used in the azimuthal and axial directions, while the expansion ratio of 1.1 is employed in the radial direction.

3- Validations

To validate the present numerical scheme a steady flow in a 90° curved pipe with a curvature radius of 24mm at a Reynolds number of 300 based on the pipe diameter of D = 8mm is considered according to the experimental set up of [38]. The axial velocity profiles in the symmetric plane at several cross sections of the curve are compared with the experimental data of [38] in Fig. 2, where reasonable agreements are observed.

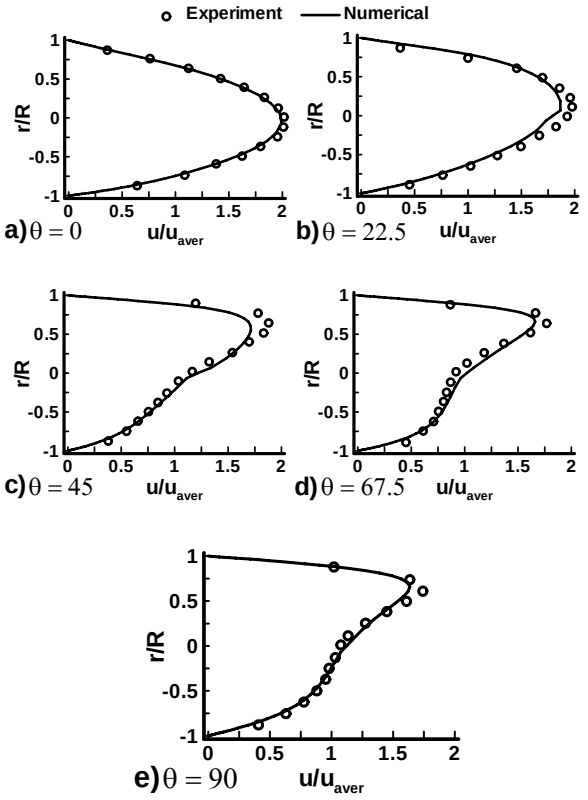

Figure 2. Comparison of axial velocity profiles with the experimental data of [38].

4- Results and discussion

To study the hydrodynamic and heat transfer characteristics of the nanofluids in a curved pipe, the axial velocity, temperature fields and secondary flows in different cross sections of the pipe for different

nanoparticles concentrations will be examined. The axial variations of the heat transfer rates and wall shear stresses, which are directly related to the pressure drop, will also be discussed at varying Reynolds and Peclet numbers. It must be emphasized that for the given effective thermophysical properties the averaged inlet velocity is adjusted to obtain constant Peclet flows for different nanoparticles concentrations.

To gain a better understanding of the curvature effects on the velocity field, the 3-D axial velocity profiles at specified cross sections shown in Fig. 2 are presented in Fig. 3. The axial velocity profiles are normalized with the averaged inlet velocity, U_{ave}, and rotated according to their actual positions in the pipe and also around the axial axis to provide their most informative views. The thermo physical properties listed in Table 1 for water and CNT are used to evaluate the effective thermophysical properties according to the relations discussed earlier. The flow Reynolds number of 1570 is considered for nanotubes concentration of 0.8%, which also corresponds to the Pe = 1000 (Pe = $U_{ave}D/\alpha_e$, where $\alpha_e = k_e/\rho_e C_{pe}$).

Clearly, the fully developed inlet profile preserves its parabolic structure throughout the inlet straight section of the pipe (cross section b). The velocity profile at the curve inlet is then slightly skewed toward the inner wall due to the curvature of the geometry (cross section c). In fact, the curve acts as an obstacle for the velocity profile just at the inlet that shifts the velocity profile slightly toward the inner wall. However, inside the curve, flow accelerates along the outer wall region of the curve due to the centrifugal forces, and the point of maximum velocity shifts dramatically toward the outer wall of the pipe (cross sections d and e) forming the secondary flows. The velocity profile reveals almost similar features in the straight section after the curve since the secondary flows are strong enough to maintain their momentum for some distance inside the straight section of the pipe (cross sections f-i).

The secondary flows, which superimposed upon the axial velocity flow field change the flow and heat transfer patterns dramatically. The fluid mixing character of the secondary flows enhances the heat transfer rates, while at the same time increases the pressure drop.

Figure 4 shows the dimensionless axial velocity contours (based on the averaged inlet velocity), secondary flows and temperature contours $(T-T_i)/(T_w-T_i)$. The results are presented at specified cross sections as shown in Fig. 2 for three different Peclet numbers of 600, 1000 and 1400 and two different values of CNTs concentrations of $\phi = 0\%$ and 0.8%. The corresponding Reynolds numbers for the considered Peclet numbers are Re ≈ 101, 168 and 236, respectively, in the case of $\phi = 0\%$, while in the case of $\phi = 0.8\%$ are Re ≈ 940, 1570 and 2200, respectively.

Table 1. Material properties

Material	Cp [J kg^{-1} K^{-1}]	ρ [kg m^{-3}]	μ [Pa s]	k [W m^{-1} K^{-1}]
water	4183	1000	0.0008513	0.6
CNT	425	2600	-	3000

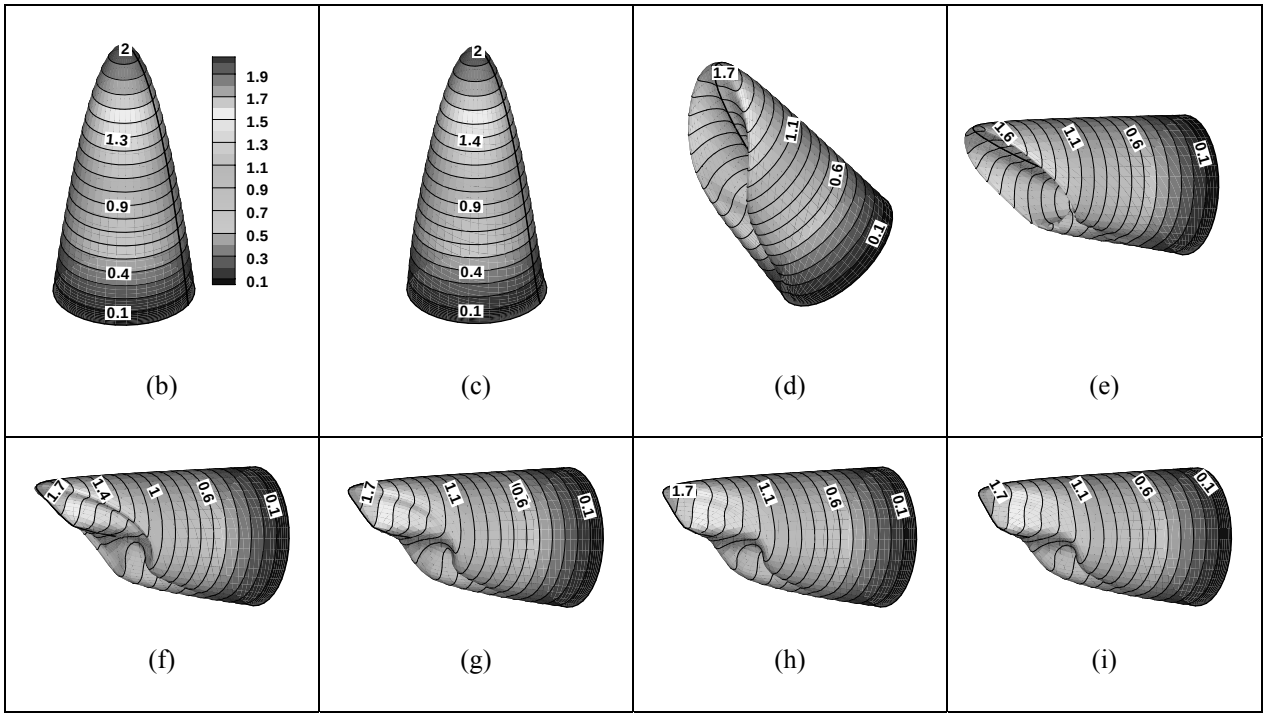

Figure 3. Axial velocity profiles at different cross sections at Pe= 1000 and $\phi = 0.8\%$ (Re= 1570)

The centrifugal forces induced by the curvature tend to push the fluid in the core region toward the outer wall of the bend, which in turn moves the fluid around the outer wall back toward the inner wall along the side walls forming a pair of symmetric counter-rotating vortices in the cross-section. Therefore the axial velocity profiles are no longer of parabolic shape. The maximum velocity point shifts toward the outer wall. The maximum intensity of secondary flows occurs around the middle of the curve (cross section d). For a given Pe, increasing the Reynolds number amplifies the centrifugal forces and consequently secondary flows. Therefore, the degree of velocity skewness increases and the maximum velocity point moves closer to the outer wall. A similar behavior can be observed by increasing the Peclet number, since it also associates with increasing Reynolds number. At higher Peclet numbers the secondary flows become stronger promoting fluid mixing and enhancing the heat transfer rate. The effect of Peclet number will be discussed in more detail later with respect to Fig. 7.

The effects of CNTs concentrations on flow and temperature fields are also shown in Fig. 4. For a given Pe, increasing the nanoparticles concentration augments the effective thermal conductivity and decreases the specific heat capacity. Therefore, molecular thermal diffusion of the nanofluid increases, leading to more uniform cross sectional temperature distributions and higher heat transfer rates, which increase the bulk temperature.

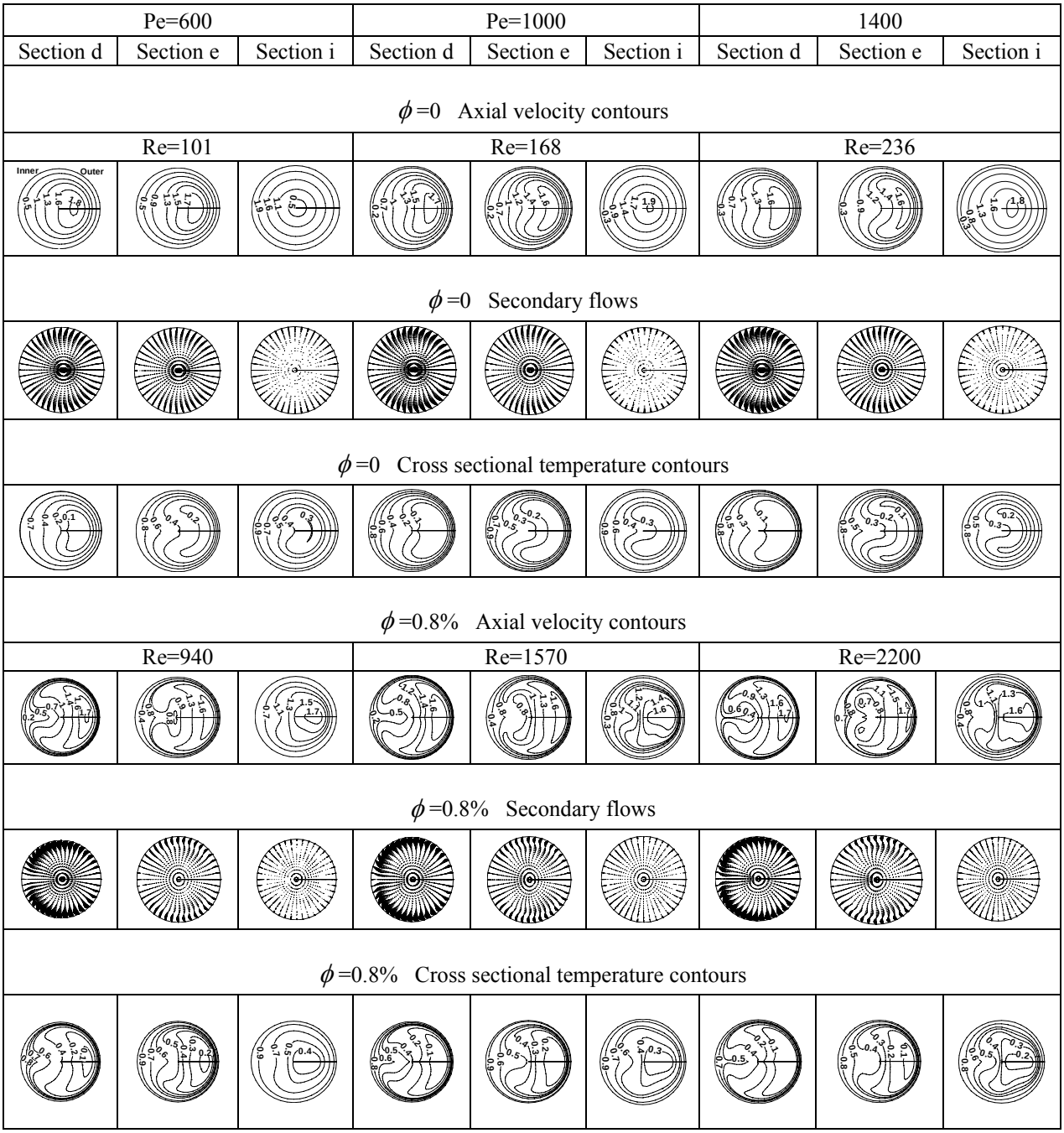

Figure 4. Axial velocity contours, secondary velocity vector fields and cross sectional temperature distributions at different Reynolds numbers and nanoparticle concentration levels

One of the important parameters associated with the pipe hydrodynamic is wall shear stresses. The wall shear stresses are the only cause for the pressure drop in a fully developed region. Furthermore, the wall shear stress distribution can identify the high risk areas for erosion in pipes. In the present study, a special form of non-dimensional wall shear stress (WSS) as defined by equation 10 is introduced.

$$WSS = \left| \frac{D\tau_w}{2\mu_e U_{ave}} \right| \quad (10)$$

here, τ_w is the dimensional wall shear stress. Wall shear stress also indicates the velocity gradients near the wall, which in turn is related to the heat transfer rate, since the increase in velocity gradients near walls causes the thermal boundary layer to decrease and consequently enhances the heat transfer rate from the wall to the fluid.

Figure 5 indicates the effect of CNTs volume fractions on wall shear stresses at Pe=600 and for three CNTs volume fractions of ϕ= 0%, 0.4% and 0.8% corresponding to the Re = 101, 560 and 940, respectively.

The wall shear stresses are stronger along the outer line of the bend and weaker along the inner line. Increasing CNTs volume fraction, which leads to higher Reynolds numbers increases the wall shear stress. As the CNTs volume fraction increases, the axial velocity profiles shift more toward the outer wall, which leads to higher wall shear stresses in this region. Locally, the wall shear stress difference between the inner and outer walls becomes more pronounced as the CNTs volume fraction increases.

As mentioned earlier, both the curvature and nanofluids are expected to enhance the heat transfer rates. To examine the simultaneous effects of these two factors the thermal fields and heat transfer rates are discussed in more detail.

First, the temperature variations along the pipe are considered for the same flow conditions as those of Fig. 3. The temperature profiles are normalized in the form of $(T-T_i)/(T_w-T_i)$. The three dimensional temperature profiles at specified cross sections shown in Fig. 2 are presented for Pe=1000 and $\phi = 0.8\%$ in Fig. 6. These flow conditions also correspond to the Reynolds number of 1570. The profiles are rotated according to their physical orientations in the pipe for clarity. In contrast to the velocity profiles, which develops from a parabolic profile at the inlet, a uniform inlet temperature profile is considered, and thus the core region of the pipe at the inlet of the curved section is still uniform.

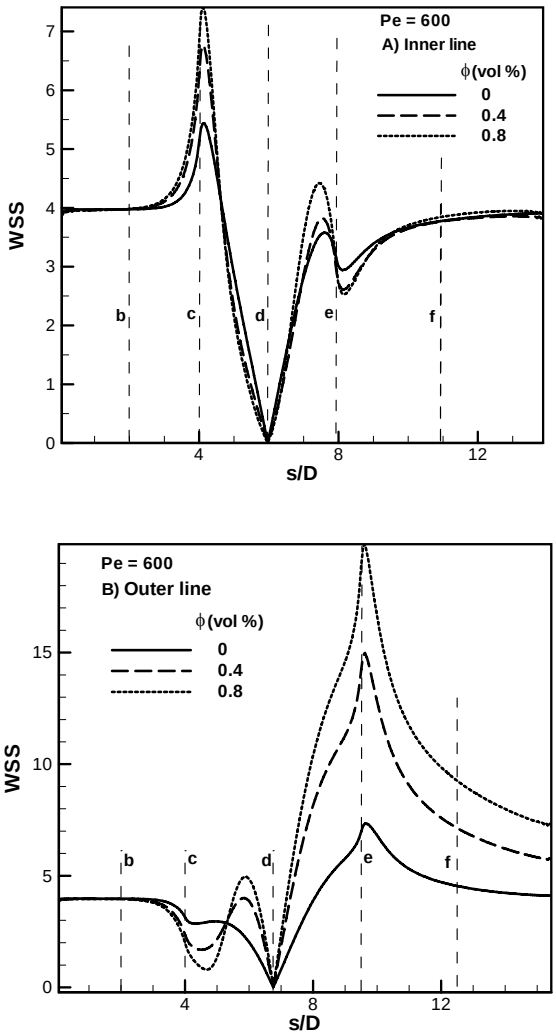

Figure 5. Axial variations of wall shear stresses along the A) inner line; and B) the outer line of the pipe

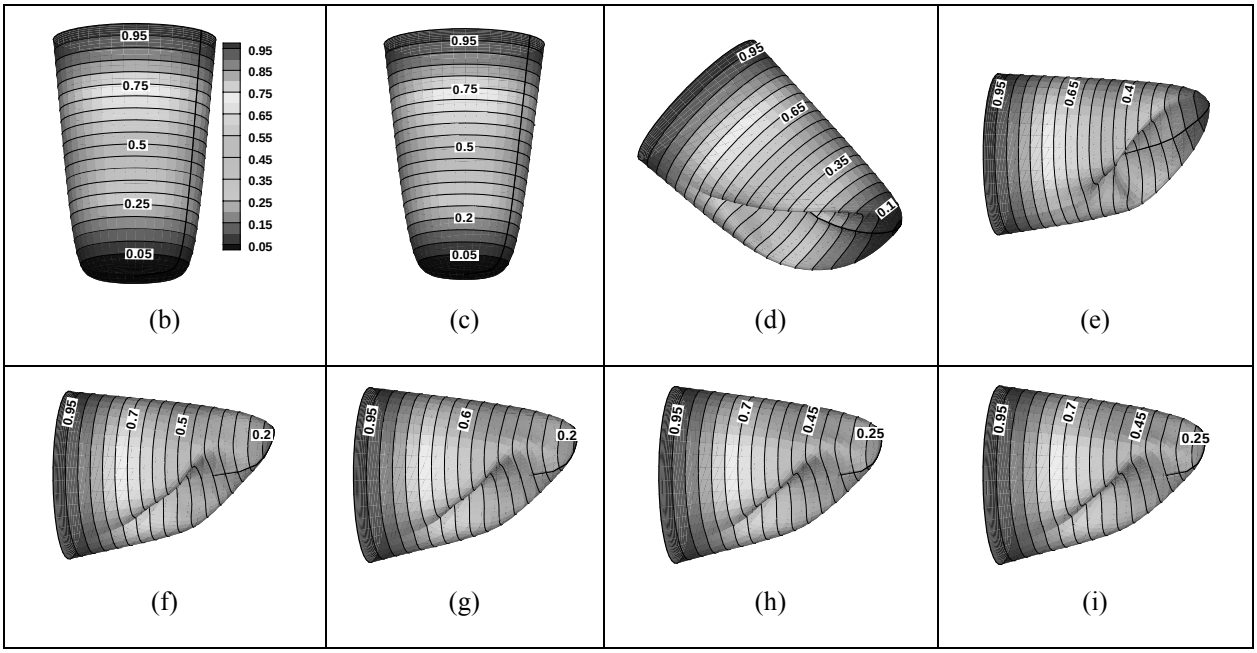

Figure 6. Three dimensional temperature profiles at specified cross sections at Pe= 1000 and $\phi = 0.8\%$ and Re = 1570

Close to the curve exit and the following straight section, where the uniform inlet effects have fairly vanished, the temperature profiles follow similar variations as those of the velocity profiles in Fig. 3. Clearly, after cross section d, the temperature gradients around the inner wall region are lower than those of the outer wall, which is accompanied by lower heat transfer rates in these regions as will be discussed later.

As discussed earlier with respect to Fig. 4, higher Peclet flows increase the strength of the secondary flows, which is reflected in the heat transfer rates as can be seen in Fig. 7. In this figure, the effect of Peclet number on the axial variations of the Nusselt number of the based fluid are examined. In the horizontal axis *s* represents the coordinate along the flow direction normalized with the pipe diameter, *D*. The peripherally averaged Nusselt number is defined as:

$$Nu = \frac{\overline{\partial T / \partial n\big|_{wall}}}{(T_w - T_m)} D \qquad (11)$$

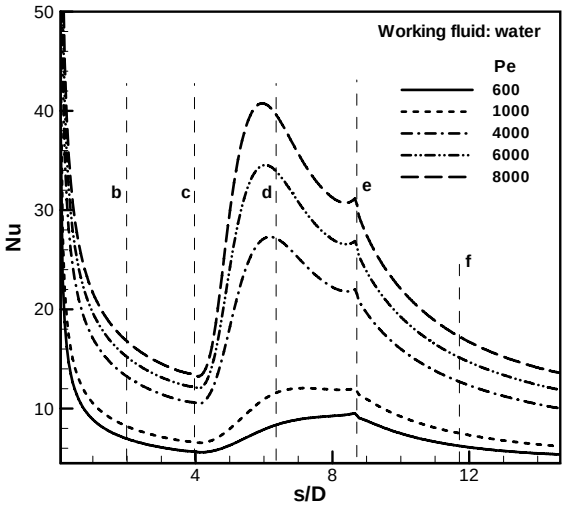

Figure 7. Axial variations of Nusselt number of based fluid flow at different Peclet numbers

Fig. 7 shows that the Nusselt number of the base fluid increases dramatically in the curved section, which is more pronounced at

higher Pe. Sharp gradients of the temperature profiles along the outer region of the curved section, as can be observed in Figs. 6c-d, account for the sudden increase in the Nusselt number from the curve inlet to about the middle of the curve. However, the decrease in the Nusselt number from the middle of the curve to the curve exit is due to the formation of the relatively low temperature gradients regions around the inner wall as can be clearly seen in Figs. 6d-e, in addition to the slight reduction in the temperature gradients along the outer wall. The slight bump that can be seen around the bend exit, which is clearer at higher Pe, is related to the reinforcement of the secondary flows at the exit due to the change in curvature from a finite value for the curved part to an infinite value of the straight pipe section attached to the exit. This sudden change in curvature locally strengthens the secondary flows, which is reflected as a slight bump in the Nusselt number variations. Beside the curvature effects, the nanofluids increase the heat transfer characteristics. Fig. 8 shows the peripherally averaged Nusselt numbers along the pipe at different values of the Peclet numbers for nanofluids with different CNTs volume fractions. The figure indicates that nanofluids further promote the Nusselt number in the curved section, which is more pronounced at higher CNTs concentrations and Peclet numbers. The behavior of the axial Nusselt number variations inside the curve section of the pipe can be explained along the same lines as those offered with respect to Fig. 7.

The axial variations of the mean nanofluids temperature, T_m, as a function of Pe and nanoparticles concentration are plotted in Fig. 9. As mentioned before, the mean fluid temperature is expected to increase with increasing CNTs volume fraction for a given Peclet number, as a higher nanoparticles concentration increases the effective thermal conductivity of the nanofluid and reduces the heat capacitance, leading to an increase in the molecular thermal diffusion of the nanofluid, which in turn enhances the mean temperature.

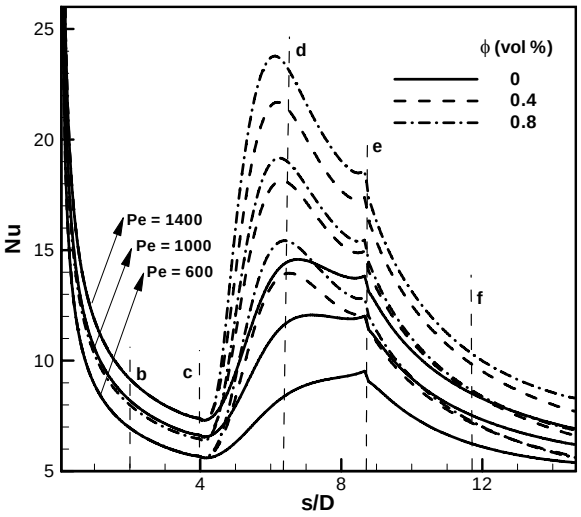

Figure 8. Axial variations of Nusselt number for different Peclet numbers and volume fractions of nanoparticles

On the other hand, for a given volume fraction of CNTs the mean temperature decreases at higher Pe. Since for constant thermophysical properties and a fixed geometry the only way to increase the Peclet number is the increase in inlet velocity. Despite the fact that higher flow velocities are associated with the higher heat transfer rates, due to the reduction of residence time of the fluid inside the tube and the larger amount of mass flow rate, the mean temperature of the fluid decreases.

It is also interesting to note that considerable increases in mean temperatures occur in the

curved section of the pipe due to the higher heat transfer rates as discussed earlier in relation with Fig. 8.

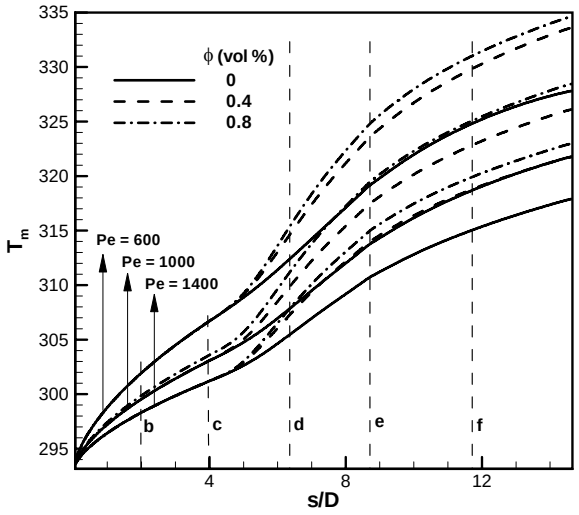

Figure 9. Axial variations of the mean temperature for different Peclet numbers and volume fractions of nanoparticles

Finally, the effects of nanoparticle concentration on the overall heat transfer rates are shown in Fig. 10. The overall heat transfer rates, $\dot{Q}$, are normalized with the heat transfer rate at Pe=600 and $\phi = 0\%$. Clearly, increasing the nanoparticles concentration similar to the Peclet number enhances the overall heat transfer rate. As mentioned earlier, keeping the Peclet number constant while the concentration level increases requires higher inlet velocities, leading to larger velocity and temperaturing gradients at walls, and consequently enhancing the heat transfer rates.

It must be emphasized that from the calculation of the overall heat transfer rate according to the equation $\dot{Q} = \dot{m}C_{p_e}(T_{out} - T_{in})$, it cannot be directly shown that the overall heat transfer rate increases at a higher Peclet number and concentrations, due to the opposing effects of these parameters on the mass flow rate, specific heat and outlet mean temperature. For a given Pe, an increase in nanoparticle concentration increases the mass flow rate and also the outlet mean temperature as indicated by Fig. 9, while decreasing the specific heat. It seems that for the case under study, the positive effects prevail over the negative effects of specific heat reduction such that the overall heat transfer rates increase at higher concentration levels significantly.

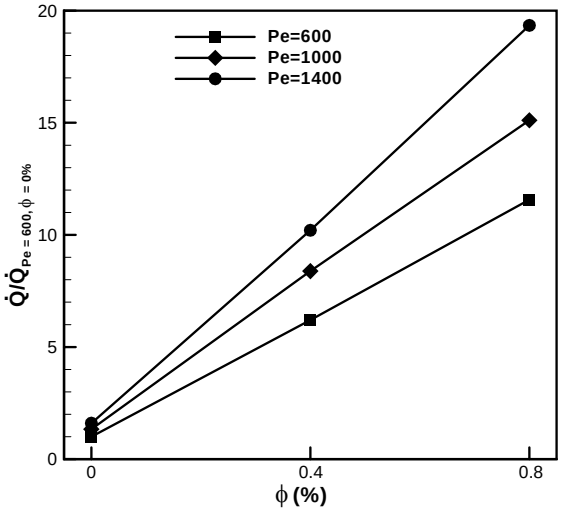

Figure 10. Overall heat transfer rates normalized by the overall heat transfer rate at Pe=600 and $\phi = 0\%$ for different Peclet numbers and volume fractions of nanoparticles

However, for a given nanoparticles concentration the specific heat remains constant, yet there are two opposing effects as the Pe increases, which are the increase in mass flow rate and the decrease in outlet mean temperature (Fig. 9). Apparently, the increase in mass flow rate is more dominant, and according to Fig. 10 the overall heat

transfer rate increases considerably at higher Peclet numbers.

5- Conclusions

In this research, two passive heat transfer enhancement techniques, which are the curvature effects and nanoparticles, are studied. The numerical simulation of steady laminar flow and heat transfer of nanofluids in a 90 degree curved pipe is considered. An interfacial layer-based model is adopted for the prediction of the effective thermal conductivity of nanofluids having cylindrical nanoparticles. This model considers the effect of a monolayer of liquid molecules at the solid particle interface. It shows that the thermal conductivity of this monolayer is much greater than bulk fluid for CNT/water nanofluid.

The axial variations of the Nusselt number and wall shear stresses are examined in detail. The results indicate that due to the secondary flow motion induced by the curvature effects the heat transfer rates are improved considerably, which is enhanced further in the presence of the nanoparticles. Yet, the gain in heat transfer enhancements is accompanied by considerable increases in the wall shear stresses, which is reflected in the pressure drop increase. Both Nusselt number and wall shear stresses go through complicated patterns in the curved section of the pipe due to the superimposing of secondary flows on the axial main stream. Increasing the concentration level of CNTs leads to larger heat transfer rates and more uniform cross sectional temperature distributions, which in turn increase the mean temperatures. Curvature and nanoparticles effects are more pronounced at higher Peclet number flows. However, at a given nanoparticle concentration the cross sectional mean temperatures reduce at larger Peclet numbers due to the higher averaged velocities and the resulting increase in mass flow rates.

Reference

[1] Naphon, P., and Wongwises, S., "A review of flow and heat transfer characteristics in curved tubes", Renewable and Sustainable Energy Reviews, 10 (5), 463 (2006).

[2] Das, S. K., Choi, S. U. S., Yu, W., and Pradeep, T., Nanofluids Science and Technology, John Wiley & Sons, Inc., New Jersey, USA, p. 4 (2007).

[3] Tillman, P., and Hill, P. J., "Determination of nanolayer thickness for a nanofluid", Int. Communications in Heat and Mass Transfer, 34, 399 (2008).

[4] Leong, K. C., Yang, C., and Murshed, S. M. S., "A model for the thermal conductivity of nanofluids – the effect of interfacial layer", J. Nanoparticle Research, 8, 245 (2006).

[5] Murshed, S. M. S., Leong, K. C., and Yang, C., "Investigations of thermal conductivity and viscosity of nano-fluids", Int. J. Thermal Sciences, 47, 560 (2008).

[6] Zhou, X. F., and Gao, L., "Thermal conductivity of nanofluids: Effects of graded nanolayers and mutual interaction", J. Applied Physics, 103 (8), 083503-1 (2008).

[7] Yu, W., and Choi, S. U. S., "The role of interfacial layers in the enhanced thermal conductivity of nanofluids: A renovated Maxwell model", J. Nanoparticle Research, 5, 167 (2003).

[8] Daungthongsuk, W., and Wongwises, S., "A critical review of convective heat transfer of nanofluids", Renewable and Sustainable Energy Reviews, 11, 797 (2007).

[9] Ding, Y., Alias, H., Wen, D., and Williams, R. A., "Heat transfer of aqueous of carbon nanotubes (CNT nanofluids) ", Int. J. Heat Mass Transfer, 49, 240 (2006).

[10] Heris, S.Z., Esfahany, M. N., and Etemad, S. G., "Investigation of CuO/ water nanofluid laminar convective heat transfer through a circular tube", J. Enhanced Heat Transfer, 13 (4), 279 (2006).

[11] Heris, S. Z., Etemad, S. G., and Esfahany, M. N., "Experimental investigation of oxide nanofluids laminar flow convective heat transfer", Int. Communications in Heat and Mass Transfer, 33, 529 (2006).

[12] Heris, S. Z., Esfahany, M. N., and Etemad, S. G., "Experimental investtigation of convective heat transfer of Al_2O_3/water nanofluid in circular tube", Int. J. Heat Fluid Flow, 28 (2), 203 (2007).

[13] Chen, H., Yang, W., He, Y., Ding, Y., Zhang, L., Tan, C., Lapkin, A. A., and Bavykin, D. V., "Heat transfer and flow behaviour of aqueous suspensions of titanate nanotubes (nanofluids) ", Powder Technology, 183, 63 (2008).

[14] Hwang, K. S., Jang, S. P., and Choi, S. U.S., "Flow and convective heat transfer characteristics of water-based Al_2O_3 nanofluids in fully developed laminar flow regime", Int. J. Heat and Mass Transfer, 52, 193 (2009).

[15] Lai, W. Y., Vinod, S., Phelan, P. E., and Prasher, R., "Convective heat transfer for water-based alumina nanofluids in a single 1.02-mm tube", J. Heat Transfer, 131, 112401-1 (2009).

[16] Anoop, K. B., Sundararajan, T., and Das, S. K., "Effect of particle size on the convective heat transfer in nanofluid in the developing region", Int. J. Heat and Mass Transfer, 52, 2189 (2009).

[17] Rea, U., McKrell, T., Hu, L., and Buongiorno, J., "Laminar convective heat transfer and viscous pressure loss of alumina–water and zirconia–water nanofluids", International Journal of Heat and Mass Transfer, 52, 2042 (2009).

[18] Buongiorno, J., "Convective Transport in Nanofluids", J. Heat Transfer, 128, 240 (2006).

[19] Maiga, S. E. B., Palm, S. J., Nguyen, C. T., Roy, G. and Galanis, N., "Heat transfer enhancement by using nanofluids in forced convection Flows", Int. J. Heat and Fluid Flow, 26, 530 (2005).

[20] Akbarinia, A., and Behzadmehr, A., "Numerical study of laminar mixed convection of a nanofluid in horizontal curved tubes", Applied Thermal Engineering, 27, 1327 (2007).

[21] Mirmasoumi, S., and Behzadmehr, A., "Numerical study of laminar mixed convection of a nanofluid in a horizontal tube using two-phase mixture model", Applied Thermal Engineering, 28, 717 (2008).

[22] Mirmasoumi, S., and Behzadmehr, A., "Effect of nanoparticles mean diameter

on mixed convection heat transfer of a nanofluid in a horizontal tube", Int. J. Heat and Fluid Flow, 29, 557 (2008).

[23] Akbari, M., Behzadmehr, A., and Shahraki, F., "Fully developed mixed convection in horizontal and inclined tubes with uniform heat flux using nanofluid", Int. J. Heat and Fluid Flow, 29, 545 (2008).

[24] Akbarinia, A., "Impacts of nanofluid flow on skin friction factor and Nusselt number in curved tubes with constant mass flow", Int.l J. Heat and Fluid Flow, 29, 229 (2008).

[25] Akbarinia, A., and Laur, R., "Investigating the diameter of solid particles effects on a laminar nanofluid flow in a curved tube using a two phase approach", Int. J. Heat and Fluid Flow, 30, 706 (2009).

[26] Haghshenas Fard, M., Esfahany, M. N., and Talaie, M. R., "Numerical study of convective heat transfer of nanofluids in a circular tube two-phase model versus single-phase model", Int. Communi-cations in Heat and Mass Transfer, 37, 91 (2010).

[27] Lotfi, R., Saboohi, Y., and Rashidi, A.M., "Numerical study of forced convective heat transfer of Nanofluids-Comparison of different approaches", Int. Communications in Heat and Mass Transfer, 37, 74 (2010).

[28] Mokmeli, A., and Saffar-Avval, M., "Prediction of nanofluid convective heat transfer using the dispersion model", Int. J. Thermal Sciences, 49, 471 (2010).

[29] Ebrahimnia-Bajestan, E., Niazmand, H., and Renksizbulut, M., "Flow and heat transfer of nanofluids with temperature dependent properties", Proceedings of ASME 2010 3rd Joint US-European Fluids Engineering Summer Meeting and 8th Int. Conf. on Nanochannels, Microchannels, and Minichannels, FEDSM2010-ICNMM2010, Montreal, Canada, (2010).

[30] Santra, A. K., Sen, S., and Chakraborty, N., "Study of heat transfer due to laminar flow of copper–water nanofluid through two isothermally heated parallel plates", Int. J. Thermal Sciences, 48, 391 (2009).

[31] He, Y., Men, Y., Liu, X., Lu, H., Chen, H., and Ding, Y., "Study on forced convective heat transfer of non-Newtonian nanofluids", J. Thermal Science, 18 (1), 20 (2009).

[32] He, Y., Men, Y., Zhao, Y., Lu, H., and Ding, Y., "Numerical investigation into the convective heat transfer of TiO_2 nanofluids flowing through a straight tube under the laminar flow conditions", Applied Thermal Engineering, 29, 1965 (2009).

[33] Chen, L., Xie, H., Li, Y. and Yu, W., "Nanofluids containing carbon nanotubes treated by mechanochemical reaction", Thermochimica Acta, 477, 21 (2008).

[34] Chorin, A.J., "Numerical solution of the Navier-Stokes equations", Math. Comput., 22, 745 (1968).

[35] Dwyer, H. A., "Calculation of droplet dynamics in high temperature environments", Progress in Energy and Combustion Science, 15, 131 (1989).

[36] Renksizbulut, M., and Niazmand, H., "Laminar flow and heat transfer in the

entrance region of trapezoidal channels with constant wall temperature", ASME J. Heat Transfer, 128, 63 (2006).

[37] Dwyer, H. A., Cheer, A. Y., Rutaginira, T., and Shahcheraghi, N., "Calculation of unsteady flows in curved pipes", ASME J. Fluids Engineering, 123, 869 (2001).

[38] Van de Vosse, F. N., Van Steenhoven, A. A., Segal, A., and Janssen, J. D., "A finite element analysis of the steady laminar entrance flow in a 90 curved tube", Int. J. for Numerical Methods in Fluids, 9, 275 (1989).